Chapter

Wear Protective Effects of Tribolayer Formation for Copper Based Alloys in Sliding Contacts: Alloy Dependent Sliding Surfaces and Their Effects on Wear and Friction

Ulrike Cihak-Bayr, Robin Jisa and Friedrich Franek

Abstract

High sliding wear resistance is generally attributed to high hardness and high mechanical strength. Novel near net shape process technologies such as metal injection moulding (MIM) or lost foam casting (LF) lack forming processes that typically increase strength. Consequently, the materials exhibit large-grained microstructures with low defect densities. Commercial copper alloys (CuSn8, CuNi9Sn6, CuSn12Ni2) well known for good sliding properties were produced using MIM and LF and characterised in the current study. Their wear and friction behaviour was compared to conventionally produced variants in a lubricated, reciprocating sliding test against steel. The results showed an equal or superior wear resistance and lower friction levels for large-grained microstructures evolving in MIM and LF. SEM, FIB and EBSD studies revealed a tribolayer on the surface and a tribologically transformed layer (TTL), composed of a nano-crystalline zone or partially rotated grains, and selective hardening of grains. The extent of the TTL was different for alloys that were chemically identical but exhibited different initial microstructures. Innovative production routes investigated here showed no tribological drawbacks, but present the potential to increase lifetime, as nano-crystalline zones may render the sample more prone to wear. We present a hypothesis on the cause for these behaviours.

Keywords: Cu-alloys, net-shape forming processes, wear behaviour, tribologically transformed layers, nano-crystalline zone, deformation induced processes

1. Introduction

Innovative technologies that enable production of new materials and complex composites unfortunately do not find their way into engineering application. This is due to a widespread, fundamental lack of trust in new materials or materials produced via non-conventional production processes [1]. With growing awareness

for limited energy and environmental resources, paired with cost aspects, innovative near net shape technologies gain interest [2]. The effects of these processing technologies on microstructural details and furthermore on friction and wear are not sufficiently understood to predict material behaviour in a sliding contact to regulate wear rates and or frictional levels. Apart from classical structural mechanical properties, these tribological characteristics have to be known for a proper design with a new material.

In the present chapter two alternative production routes are evaluated for three copper based alloys. The near net shape technologies metal (powder) injection moulding (MIM) and lost foam casting (LF) are described in part 2, both are known for steel [3] and aluminium [4] but have not been commercialised for copper-based alloys and lack substantial basic knowledge in published literature. Yet, near net shape technologies are especially interesting for copper-based alloys due to the high raw metal costs. Here, a special focus is put on the characterisation of wear and friction in a lubricated sliding contact of representative alloys shown in part 3.1. The chosen experimental set-up is depicted in part 3.2 and their tribological and analytical results in part 4. Based on the observations of a formed tribolayer and the nano-crystalline zones forming a tribologically transformed layer (TTL) as described in part 4. Part 5 forms the discussion that links the findings to literature and suggests a hypothesis for the formation of tribolayer and TTL and their effect on wear and friction levels. Finally, the chapter finishes with a conclusion in part 6.

2. Copper-based alloys as tribomaterials

Copper alloys are materials with a good track record for tribological applications comprising pronounced sliding. However, the demand of alloys is limited by high raw material costs and traditional energy intensive production routes; such as melt metallurgy, casting, hot and/or cold forming; the subsequent machining processes lead to large amounts of chips that have to be collected and re-melted to be recycled. As consequence, the production of components made of copper-based alloys demand excessive energy and consequently result in high ecological impact and costs.

Energy-efficient technologies offer economical production methods and additionally large options for complex component shapes. Currently, additive manufacturing and near net shape manufacturing are the main avenues towards achieving these goals. **Figure 1** depicts a schematic of the processes involved: MIM and LF

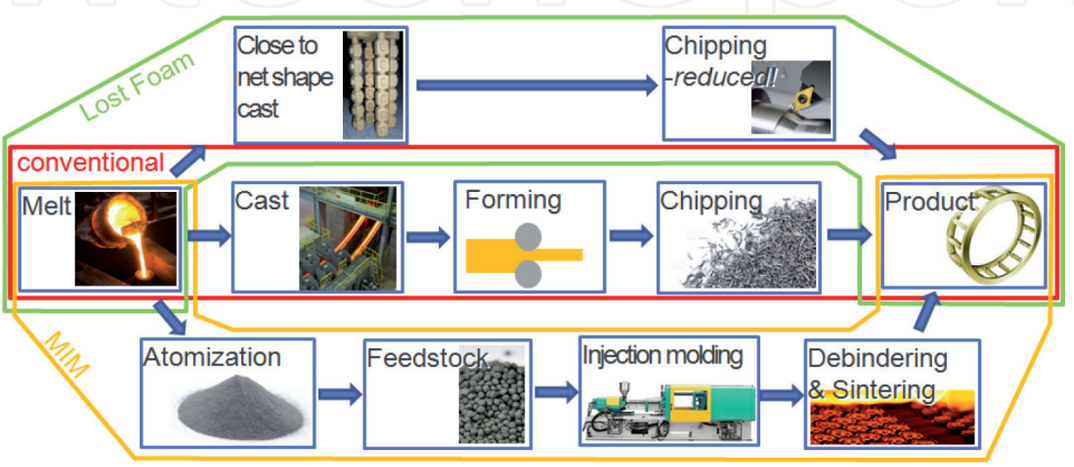

Figure 1.
Technological paths of the analysed materials.

production technologies; the basic principles are described in [5]. Such innovative production technologies usually result in different material properties compared to traditional production methods; the functionality of the component produced by alternative processes are often perceived to be inferior. For a more widespread application of new production technologies, a prediction of the target properties would be necessary. Since a correlation between the material structure and the resulting properties are not trivial, the material selection process is still mainly based on empirical knowledge of engineers. For tribologically loaded components the material selection usually relays on bulk material properties and the assumption that the harder material is the more wear resistant, which is conformed in many cases. This material rating is based on the well-known Archard's wear law [6], which correlates wear volume inversely with hardness.

Tribological studies in the nineties, have revealed that ductile alloys form an altered, fine-grained microstructure in the volume just beneath the sliding contact area as published by Rigney in [7]. Following classical approaches of material hardening, the material increases in strength as the grain size decreases and according to Archard's wear law this results in lower wear.

Most published tribological sliding experiments studying material changes were carried out on pure metals, such as Au or Cu, in a ball on plate configuration in dry contact [8–10]. They show the formation of a microstructure with much finer grain sizes compared to the initial grain size, which is only preserved in the bulk. Some studies can be found on alloys, e.g. steel [11, 12] or Co-based alloys [13, 14], which revealed grain refinement beneath the surface, too. Recent tribological studies focus on the evolution of microstructural changes such as [9, 13], but correlations of grain-size to properties e. g. strength or work-hardening are treated by material science studies: Studies on work-hardening behaviour due to grain size changes, as described for copper by [15], do not deal with grain refinement processes exhibited by tribological contacts. Besides, the strength increasing effect of refinement according to Hall–Petch relations was reported to apply until a gain size of approximately 10 nm is reached for copper [16].

Usually, superior wear resistance is attributed to those newly formed structures [13, 14], but often no explicit correlation to wear or friction is given [9]. Thus, the effect of microstructural changes in subsurface regions in a sliding contact on wear and also friction levels is not really understood and often underrated. Classical material selection strategies follow the idea that material with higher strength exhibit higher wear resistance.

3. Experimental

3.1 Investigated material

The current study compares three copper-based alloys, each produced via two different process technologies – one conventional technology route via casting, forming and machining and a near net shape new technology. The alloys are listed in **Table 1** together with their hardness values and the range of grain sizes observed in the cross sections. The microstructures resulting from different production routes are shown in **Figure 2**. The wrought alloys CuSn8 and CuNi9Sn6 are typically continuously cast, followed by forming (pressing, drawing, rolling) and, for CuNi9Sn6, heat treatment through spinodal decomposition [17]. Apart from the spinodally forming precipitations, which cannot be observed in SEM images, this alloy also forms γ precipitations (in different crystallographic structures as described in [18]) that are several μm large and are visible in SEM pictures. In light

Material	Technological route	Grain size	Hardness
CuSn8 conv.	Continuous cast, drawing, heat treatment, chipping	< 20 µm	238 HV1
CuSn8 MIM	Injection moulding, debindering, sintering	100–150 µm	70 HV10
CuNi9Sn6 conv.	Continuous cast, rolling, heat treatment, chipping	~ 50/150 µm	180 HV1
CuNi9Sn6 MIM	Injection moulding, debindering, sintering	~ 200 µm	171 HV10
CuNiSn6 MIM, heat treated 1 h@450°C	Injection moulding, debindering, sintering, heat treatment	~ 200 µm	266 HV1
CuSn12Ni2 conv.	Continuous cast, chipping	~ 50 µm	115 HB30 2.5
Cuni12Ni2 LF	Lost foam cast, chipping	Dendrite length > 500 µm	90 HB30 2.5

Table 1.
Characterised copper-based alloys and the grain sizes and hardness for different production routes of nominal identical alloys.

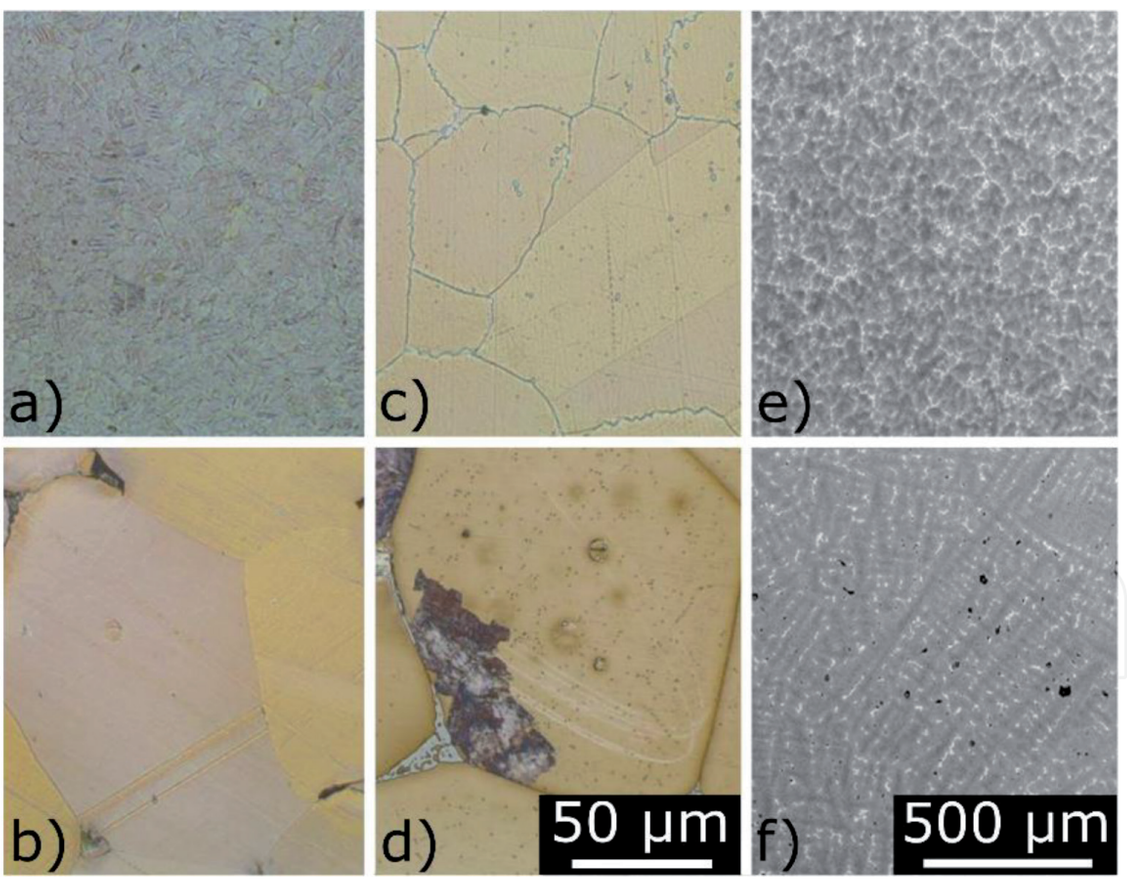

Figure 2.
Microstructures of studied alloys: Conventional: a) CuSn8 c) CuNi9Sn6 e) CuSn12Ni2; MIM: b) CuSn8, d) CuNi9SN6; LF: f) CuSN12Ni2.

microscopy images, their effects on the microstructure can be observed by grain boundary faceting as well as formation of violet lamellar phases during annealing.

Alternatively, these two alloys can be produced by a metal injection moulding (MIM) process from pre-alloyed feedstocks. The MIM production route inherently lacks a forming step and thus any possibility for grain refinement. As a result, the

average grain size of the materials produced through MIM is much coarser than the one obtained via conventional routes. **Figure 2** shows representative microstructures of all studied materials. The MIM version of CuNi9SN6 can be heat treated in the same way as the conventional version in order to increase the mechanical strength by precipitation hardening.

Continuous casting (CC) followed by machining is a typical production route for the cast alloy CuSn12Ni2. An alternative, innovative production route, which can help to save energy is a sand casting process called lost foam (LF) casting [4]. The dendritic structure resulting from LF casting is pronouncedly coarser than the CC variant as it is basically a sand-casting process with correspondingly long cooling times and lacking deformation during solidification.

All production variants of the advanced technologies, MIM and LF, lead to larger grain sizes with hardly any defects such as twins. Therefore, these material variants are significantly softer than their counterparts from the conventional production route. As often higher wear resistance is associated with high mechanical strength, the small-grained, conventionally produced alloys are expected to exhibit better wear resistance. This assumption, which is a commonly used basis for design and material choices in mechanical engineering, is verified in the current study for three alloys and two innovative production routes.

3.2 Experimental tests - tribological characterisation

Samples of the different alloy variants were studied in a lubricated reciprocal sliding contact with a modified SRV® test rig. The setup is described in more detail in [19–21]. **Table 2** summarises the main test conditions. Each set of parameters was repeated at least twice. The base oil SN150 was used for CuSn8 and CuNi9Sn6, for CuSn12Ni2 a fully formulated mineral oil, a commercial gear oil, was applied. Thus, one has to be aware of the effect of different viscosities. In order to increase wear of the fully formulated system, CuSn12Ni2 was also examined at a normal load of 240 N. These external conditions differ because the potential applications of the two technologies are different.

The friction coefficients were continuously recorded at a rate of 1 Hz and the data of individual test runs were averaged. Wear scars were characterised after the tests by topographic analysis using confocal microscopy with a Leica DCM3D at 20× magnification, which allowed the measurement of the wear track width. Afterwards, the wear volume was calculated as described in [20].

A wear map is used to illustrate the performance of the individual materials and their variants. It shows the wear volume measured at the end of the test run versus the coefficient of friction at a test time of 90 min, which corresponds to SRV standards [22]. This kind of diagram enables a simple but informative tribological rating, as both friction and wear behaviour are usually relevant. The desired low friction sliding material with a high lifetime can be found in the left lower corner.

3.3 Microstructure analysis

In order to understand modification processes deriving from tribological interactions selected samples were investigated further with light microscopy, nanoindentation, scanning electron microscopy (SEM) and focused ion beam (FIB) cross sections or electron back scatter diffraction (EBSD). EBSD was performed on cross sections normal to the sliding plane with a Zeiss Supra 40VP instrument equipped with an EBSD system from EDAX. The samples were chemically etched prior to the scan. The step sizes (0.20 μm for CuSn8 MIM; 0.10 μm for conventional CuSn8) and the scan areas (100 × 250 μm/19 × 30 μm) were adapted to the grain

Cylinder	Disc	Stroke	Frequency	Normal force	Test duration	Sliding distance	Lubrication	Disc temperature
mm	mm	mm	Hz	N	h	m	—	°C
∅ 4.2 l = 12	∅ 24 l = 7.8	3	30	100 or 240	2	1296	oil drop	50

Table 2.
SRV test parameters.

sizes of the respective samples. Scan sizes of 200 nm were chosen for CuSn8 MIM and 100 nm for conventional CuSn8. The position of the scan along the contact area was pre-selected in SEM images. Three scans were performed on a total area large enough to be representative for the largest grain sizes found in CuSn8 MIM. For microstructures like the conventionally produced CuSn8 a scan directly at the surface was not possible due to the high local deformation. A sufficient Kikuchi pattern quality was only detectable in a depth of 1 μm below the surface. The scans were analyses based on pattern quality images overlaid with the small (SAGB) and large angle grain boundaries (LAGB) as well as on the inverse pole figure (IPF) pictures with the projection direction <100>, which is the surface-normal direction to the plane of the cross section. Numerous precipitations in the MIM version of CuNi9Sn6 complicated the pattern recognition and therefore EBSD scans were omitted. FIB cuts were employed for the deeper analysis of the cast alloy CuSn12Ni2. The FIB cuts were oriented normal to the sliding direction as a cut in the sliding direction would either be located on top or at the bottom of a groove produced by wear debris.

4. Tribological behaviour

Figures 3 and **4** show the frictional behaviour over test time for all studied materials. All friction coefficient curves – except CuSn8 – are at their maximum during running-in, which ranges from 5 to 30 min. All curves end in an almost constant steady level for the chosen test duration and have thus reached steady-state conditions.

The observed friction coefficient values lie between 0.20 and 0.42. These values represent the arithmetic mean of the friction coefficients of different test runs. The data of each run was averaged for each recorded friction value, these mean values are shown as the friction curves in **Figures 3** and **4**. In order to add the information of the scattering of the individual runs for a better interpretation of the friction behaviour, the standard deviation of the friction signal of each run was calculated. The error bars in **Figures 3** and **4** represent the mean standard deviations of individual test runs with the same material, shown only every 5 min for the sake of readability,

The levels of the friction coefficients as well as the friction behaviour differ distinctly for the two materials CuSn8 and CuNi9Sn6. Their sensitivity to variations in the process route seems to be pronouncedly different, as well.

For both materials, MIM manufacturing leads to lower friction coefficients after the run-in phase. For CuSn8 the reduction is roughly 0.08, for CuNi9Sn6 it is less pronounced, namely 0.02–0.03. A heat treatment, which increases the structural strength of the CuNi9Sn6 MIM variant, further reduces the friction coefficient by about 0.07 compared to the conventionally produced CuNi9Sn6.

The MIM variant of CuSn8 shows a high variability throughout the whole test time and after an initial increase to 0.40 smoothly decreases to 0.30 between 30 min and 100 min. The values of the conventional CuSn8 lie within the variability of the MIM variant, but do not show the same characteristics over time. After an initial increase, the friction reaches an almost constant level at 0.40, which is on the upper bound of the scatter of the CuSn8 MIM data. As, the noise of conventional CuSn8 is much smaller than the MIM sample, the different levels of friction of the two CuSn8 variants are regarded as significant.

The error bars largely overlap for the conventional and the MIM version of CuNi9Sn6, indicating just a small tendency for higher average friction levels for the conventional variant. However, the run-in period is distinctly different with

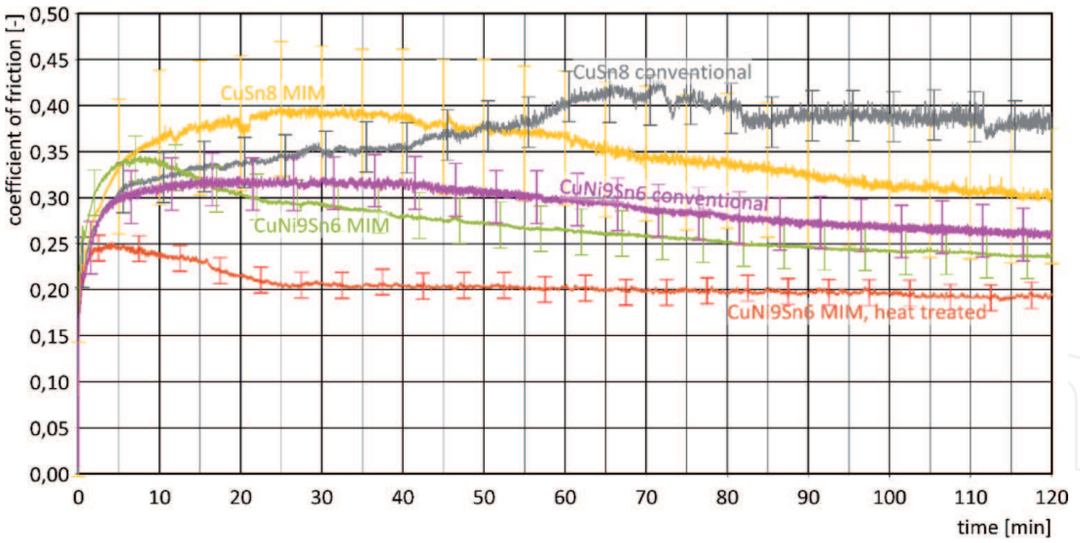

Figure 3.
Friction coefficient of CuSn8 and CuNi9Sn6 both conventionally produced and via the MIM route.

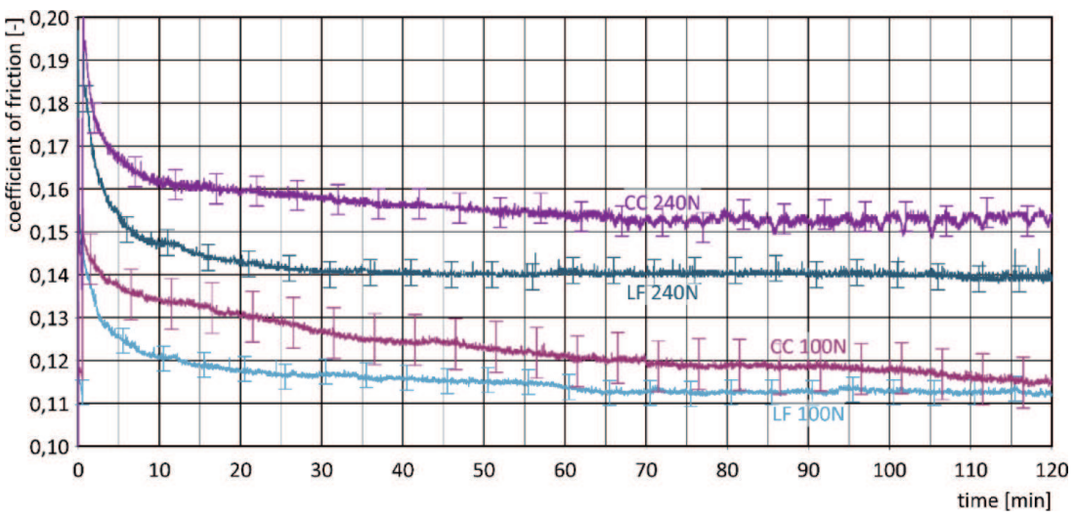

Figure 4.
Friction coefficient of CuSn12Ni2 produced via conventional casting (CC) and via lost foam cast (LF) for 100 N and 240 N normal load.

a pronounced increase for the MIM version, but lasting only 30 min, whereas the conventional material increases and decreases smoothly, reaching a steady state level just before the test ends. The characteristics of the friction curve over time seems to be unaffected by the microstructural changes during heat treatment, as there is again a steep but short increase during run-in. However, the scatter of the friction data is reduced by the heat treatment.

The averaged friction values at a test time of 90 min are depicted in **Figure 5** together with the averaged wear volume at the end of the test in a wear map. The error bars of the coefficient of friction are equivalent to those in the friction curves (**Figure 3**), the uncertainty of the wear volume is the standard deviation of the wear volume at the end of the test. The measured uncertainty is in some cases so small that it is nearly invisible in an appropriately scaled wear map.

The results illustrate a pronounced decrease of wear when the CuSn8 is produced via MIM instead of conventionally. There is also a reduction in wear for CuNi9Sn6 when comparing conventional to MIM in the heat-treated condition, but this decrease is far less pronounced. Between MIM and conventional samples there is no significant change in wear results.

For CuSn12Ni2 the friction coefficient levels are lower, ranging between 0.11 and 0.14 (**Figure 4**). This can mainly be attributed to the fully formulated gear oil used in this study, which was chosen because the tribosystem should be as close to the real application as possible. Therefore, a direct comparison between all the materials discussed before is not permissible. The differences in terms of friction between continuous and lost foam cast variant are little and judged to be irrelevant for applications. Still, the level of coefficient of friction is significantly lower for LF if the contact pressures are increased. Nevertheless, none of the two variants seems to be more sensitive to normal pressure changes than the other. More pronounced differences can be observed in the wear behaviour (**Figure 6**) of CuSn12Ni2, where the LF microstructure shows significantly lower wear volume.

For all investigated materials, the innovative production routes lead to lower wear despite weaker mechanical properties, certainly the degree of improvement depends on the alloy, **Figures 5** and **6**. There are large differences in the final wear volume between the two production routes for CuSn8, which exceeds by far the measurement uncertainty of wear. For CuNi9Sn6 the effect of the production route is much smaller but the heat-treated MIM version shows a distinct wear reduction

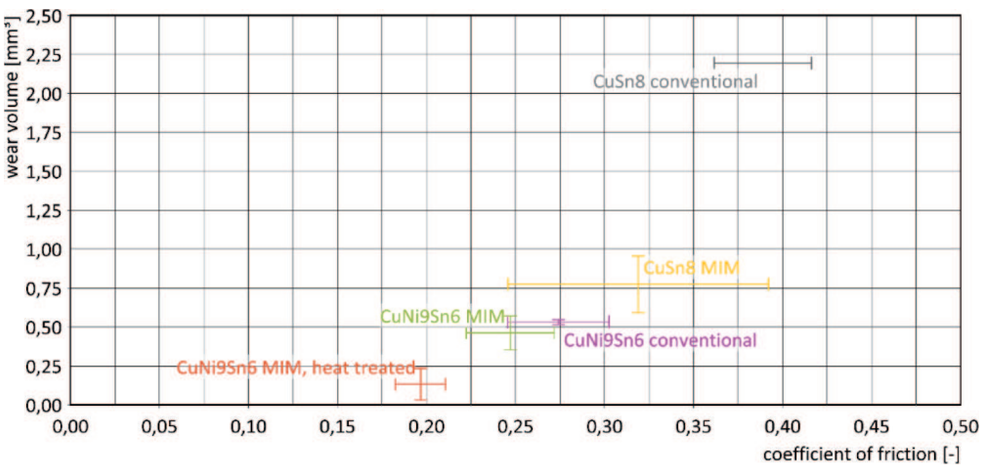

Figure 5.
*Wear map of CuSn8 and CuNi9Sn6 in two production variants: Conventional and MIM. The depicted friction coefficient was taken at a test time of 90 min and the error bars are identical to those depicted in **Figure 3**, the wear volume represents the value at the end of the test and the standard deviation of the measured volume.*

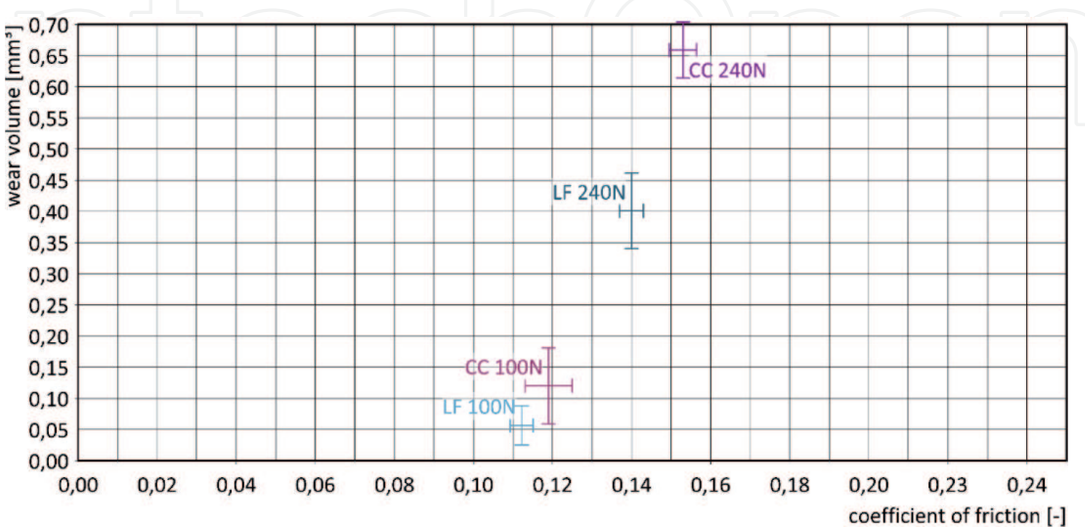

Figure 6.
*Wear map of CuSn12Ni2 produced via conventional casting (CC) and via lost foam cast (LF). The depicted friction coefficient was taken at test time of 90 min and the error bars are identical to those depicted in **Figure 4**, the wear volume represents the value at the end of the test and its standard deviation.*

compared to the conventionally produced sample. Consequently, the increase in mechanical strength due to precipitations does not impair the tribological performance, as it does reduce wear and friction levels. Heat treatment reduced the scatter of the observed friction coefficient level. The results of other samples treated at other temperatures or for different times are not shown here as the wear and friction results nearly coincide for all established heat treatment cycles. In any case, the heat-treated MIM CuNi9Sn6 version offers the lowest wear and friction among the investigated materials lubricated with mineral base oil. The initial microstructure affects the measured wear volume even within systems using additivated oils, which reduces the measured wear volumes due to a tribolayer, forming also in bronze surfaces. Again, the new casting technology (LF) variant of CuSn12Ni2 shows a better performance than the continuous cast one. The effect of different material structures becomes more pronounced for higher normal loads as can be seen in **Figure 6** for 100 N and 240 N. The effects on friction levels are lower than for the systems shown in **Figure 3**, but interestingly the noisiness of the friction coefficient reduces if the structure gets coarse and more dendritic. The latter observation seems to be independent of the applied normal load.

4.1 Tribologically induced changes in the microstructure

The higher wear resistance of softer variants of the respective alloys was initially not expected as hardness is often associated with wear resistance. As the testing conditions were identical, we investigated the microstructure in order to examine the different wear behaviour observed. The idea was that the grain and/or defect structure evolving during the sliding contact is different for these samples. As all other factors were identical, the near surface microstructure behaviour can potentially explain the differences in the macroscopic wear behaviour as well as the observed frictional levels. The light microscopy images in **Figure 7** reveal that no resolvable changes in the microstructure beneath the contact surface occur. Only

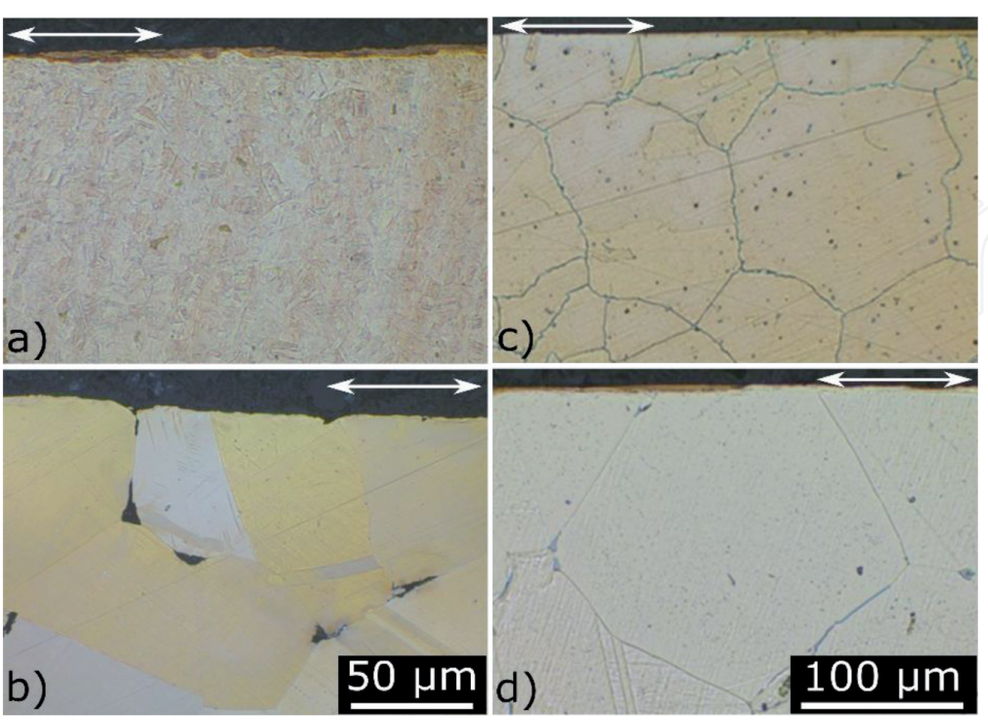

Figure 7.
Light microscopy images of cross sections of the cylindrical samples normal to the sliding direction. a) CuSn8 conventional b) CuSn8 MIM c) CuNi9Sn6 conventional d) CuNi9Sn6 MIM; the 50 µm scale applies to a) and b), the 100 µm scale to c) and d).

the MIM CuSn8 sample exhibits local increase of twins and shear bands in the first layer of grains up to a depth of 20 μm beneath the contact plane.

The LF cast structure does show defects in the light microscopy images (**Figure 8**), such as bent slip lines as well as deformation twins, which are bent additionally. The deformation is very inhomogeneous and many dendrites show no or hardly any changes visible in light microscopy images. The details in **Figure 8b** illustrate pronounced effects in the vicinity of pores. If features of plastic deformation can be observed by light microscopy images, they will reach up to depths of at least 50 μm.

The higher resolution SEM images of the cross sections shown in **Figure 7** are given in **Figure 9a** and **b** for the conventional variants and in **Figure 9c** and **d** for the MIM samples. The CuSn8 is highly twinned and some twins are bent in sliding direction. This occurs not only in the surface grains but also in grains located in deeper zones. Still, the SEM picture is not sufficient to be able to judge if these features are caused by the sliding contact as the initial structure is highly twinned already. In the higher alloyed CuNi9Sn6 the grains are larger compared to CuSn8 conventional and no features indicating deformation close to the surface are visible. The edge is very rounded due to polishing and etching prior to EBSD measurements.

In contrast to the two conventionally produced samples, both MIM alloys revealed the formation of a layer on top of the initial microstructure with a

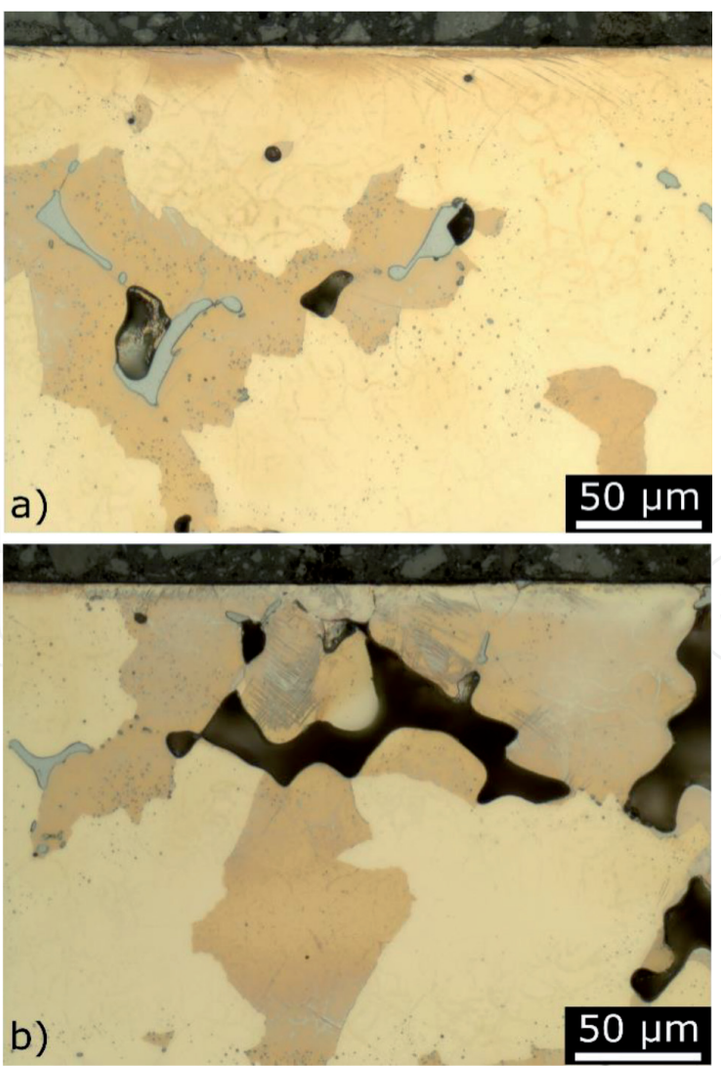

Figure 8.
Light microscopy images of cross sections of the cylindrical CuSn12Ni2 LF samples normal to the sliding direction a) and b) show two position within the same sample, in a) slip lines and in b) deformation twins in the first row of grains are visible.

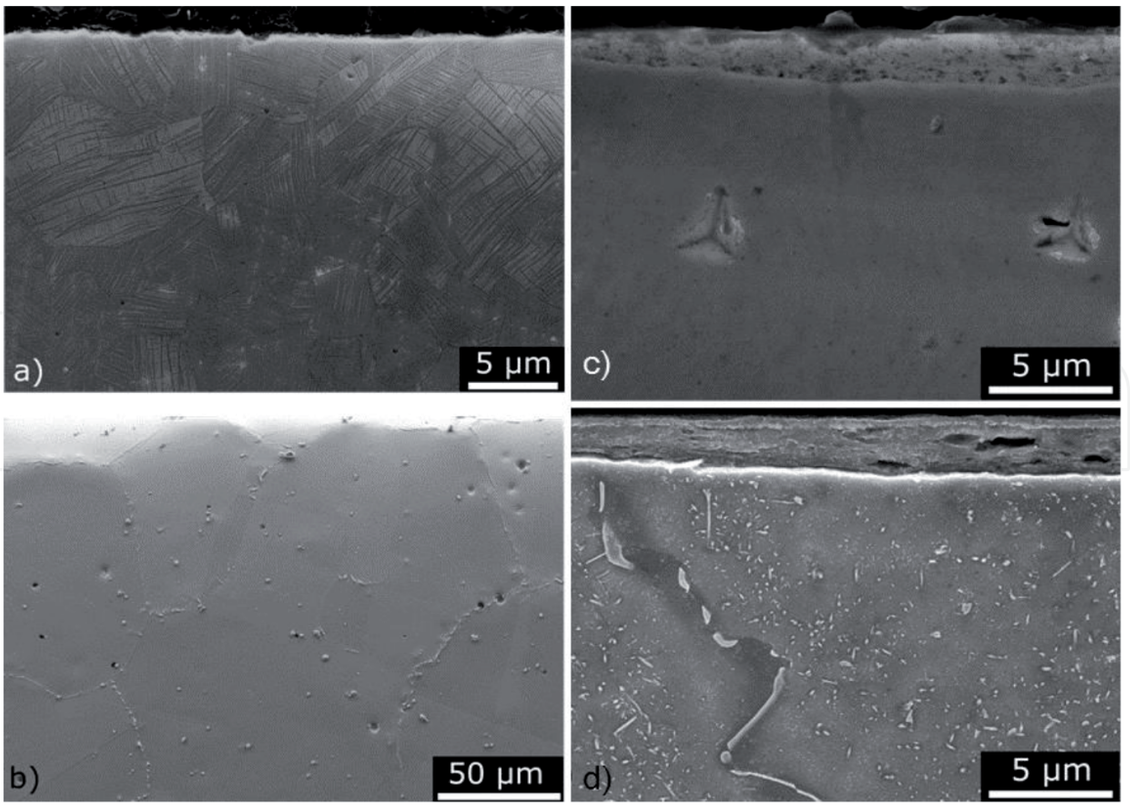

Figure 9.
SEM image of the edge zone on cross-sections oriented parallel to the sliding direction: a) CuSn8 conventional, b) CuNi9Sn6 conventional, c) CuSn8 MIM (mechanically mixed layer, 2 visible nano-indenter marks), CuNi9Sn6MIM (mechanically mixed layer lying and facetted grain boundary with γ precipitations is vertically inclined on the left side of the image).

thickness up to 2–3 µm. This feature was only observed on the MIM microstructures of the studied alloys.

The observed layer seemed to have a patch-like structure as it did not cover the whole length of the cross section. On top views of the contact area these layers were not clearly distinguishable from the rest of the microstructure, thus their size and extent of coverage cannot be given. The EDX measurements (**Table 3**) shows increased contents of oxygen and carbon and some iron. This indicates a mixture with debris from the counter-body, even though the structure appears amorphous or extremely fine-grained. However, no grain structure was resolvable with SEM. What is observable in the SEM images are pores within this layer, which are more pronounced for the layer observed on CuNi9Sn6. In the following, we refer to it as a mechanically mixed layer in order to distinguish it from the TTL, a zone comprising of defects like the slip lines and deformation twins extending over up to 20 µm as seen in **Figure 7c**.

4.2 EBSD as a tool to reveal tribologically induced changes in the microstructure

With the EBSD technique grain orientations and local misorientations can be revealed. Thus, microstructural defects like internal stresses stored in grains or the formation of subgrains and local misorientations can be detected, which cannot be observed with SEM images [23, 24]. As the changes in wear volume were most pronounced for CuSn8, the EBSD analysis focused on this alloy.

For the conventionally produced CuSn8 the forming in the production process resulted in a highly deformed and small-grained structure and any further deformation caused due to the tribological contact is not clearly visible in the SEM

images. The pattern quality picture and the IPF picture of an EBSD scan with 1 μm distance to the surface are given in **Figure 10**, with the upper edge of the scan in sliding direction. The quantitative analysis of the grain boundary lengths of large angle grain boundaries (LAGB) and small angle grain boundaries (SAGB) overlaid onto the pattern quality image indicate no increase closer to the surface and so they are not shown. However, the twin density within the first 15–20 μm appears to be higher as numerous micro-twins form. Especially in the first 5 μm, the grains are strongly elongated parallel to the sliding direction. Generally, the grain size is easier to see in IPF images and they reveal high intragranular strains by different shades of colours in nearly all grains, independently of their location with respect to the surface. Hence, internal lattice rotations do not seem to increase close to the contact but are a result of the high deformation during production. Comparing the IPF image of the initial structure to the one at the surface indicates a tendency to slightly smaller grains sizes in the first 15 μm. However, the change in size is far less pronounced than the change in shape.

Thus, the microstructure of conventional CuSn8 can hardly adapt to the stresses accumulated during sliding and has little work-hardening capability. So presumably the microstructure is just worn off soon after the initial contact during the sliding process and cannot form a wear resistant subsurface zone.

The MIM version of CuSn8 was very large grained and therefore investigated by two closely situated EBSD scans situated close together, shown in **Figure 11**.

	C	O	Si	S	Sn	Fe	Ni	Cu
At %	54.58	6.16	1.07	1.90	0.62	0.31	3.33	32.03

Table 3.
EDX analysis of the layer observed on CuNi9Sn6 in the MIM version as shown in **Figure 9c**.

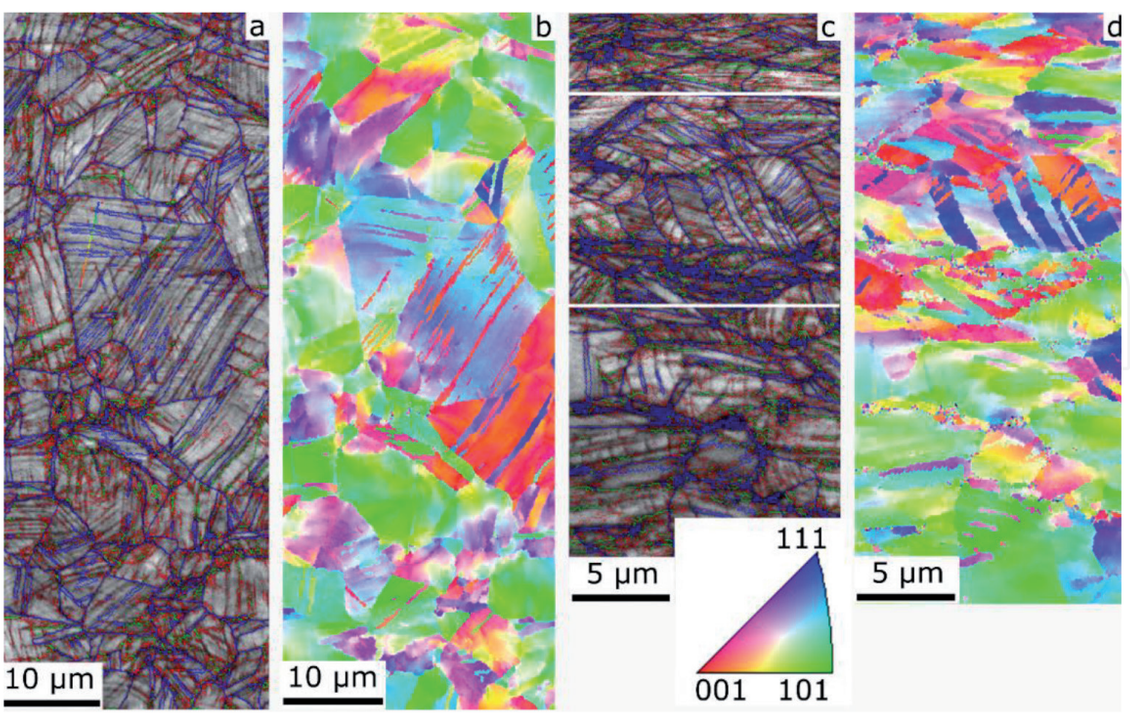

Figure 10.
CuSn8 conventional samples with the sliding direction is parallel to the upper edge. EBSD scan at a depth of 1000 μm beneath the surface: a) pattern quality image with LAGB in blue, SAGB in red and b) IPF image EBSD scan at a depth of 1 μm beneath the surface: c) pattern quality image with LAGB in blue, SAGB in red d) IPF image.

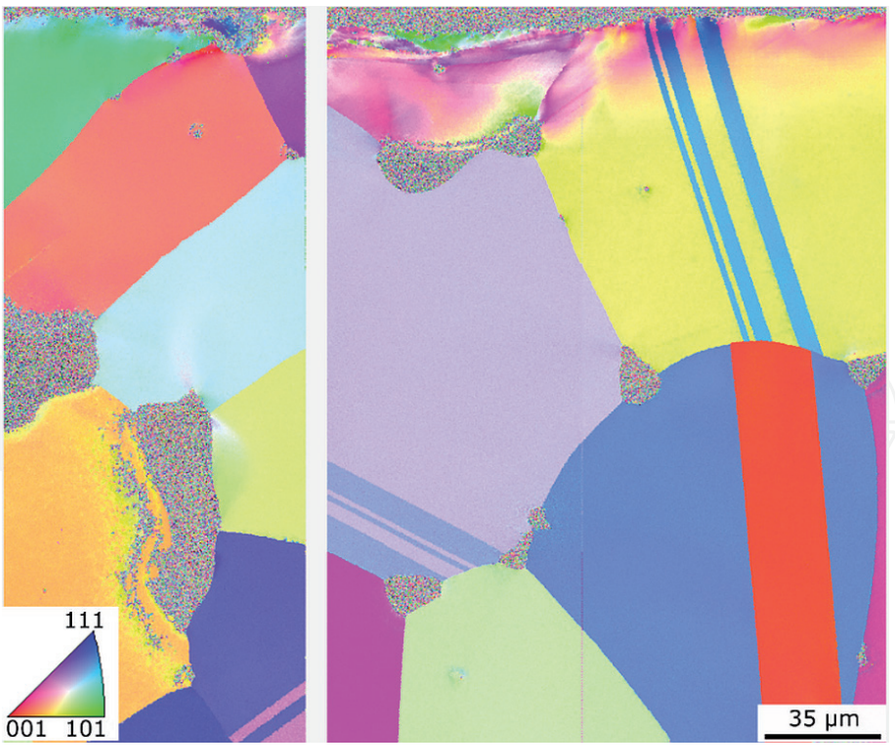

Figure 11.
CuSn8 MIM EBSD scan.

The initially undeformed MIM structure of CuSn8 shows some grains like the green coloured ones the left with no deformation features, but the grain on the right changes its orientation from yellow to pink which indicates a partial lattice rotation and an internal stress field. The respective stress field does not extend over the whole grain but is localised in the first 20 µm beneath the contact and does not affect the twin. In the middle, there is a pore close to the surface and the remaining grain located above this pore seems to be most suitable for storing plastic strain generated by the tribological sliding process. It has various shades of pink and is not as uniformly coloured as non-affected grains. The analysis of small- and large-angle grain boundaries showed no additional information and a figure was therefore omitted. Based on our observations there is no indication for an interrelationship between local lattice rotations and the position of the mechanically mixed layer lying on top of the tribo-contact area.

In addition to SEM and EBSD scans, some apparently affected grains were investigated with nanoindentation, the results of which are given in **Figure 12**. The defect structure shows a high local concentration of defects that lead to an increase in hardness by 1–1.5 GPa over the first 20 µm beneath the surface. However, grains that show no orientation changes in the EBSD scan also showed no hardening in the nanoindenter measurement.

The modulus of elasticity was quantified during nanoindentation and turned out not to vary with distance from the contact surface and is thus not given in **Figure 12**. Altogether, the results of the MIM sample suggest that if grains are modified due to the sliding process they have to be located directly at the surface, grains further away from the contact are unaffected in any case, but even at the surface many grains do not adapt by e.g. lattice rotations.

The cast alloy CuSn12Ni2, though tested with additivated oil, showed smaller but significant differences in the wear volumes of CC and LF cast samples. The tribo-surfaces had different characteristics, which are illustrated in **Figure 13a** and **b**. The surface exhibits grooves, presumably formed by wear debris, but resembles a

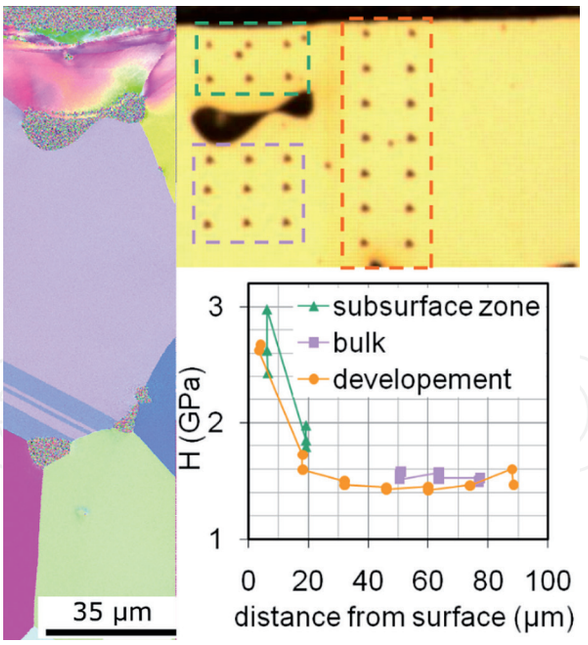

Figure 12.
Location and gradient of the nano-hardness measurements performed on the MIM version of CuSn8.

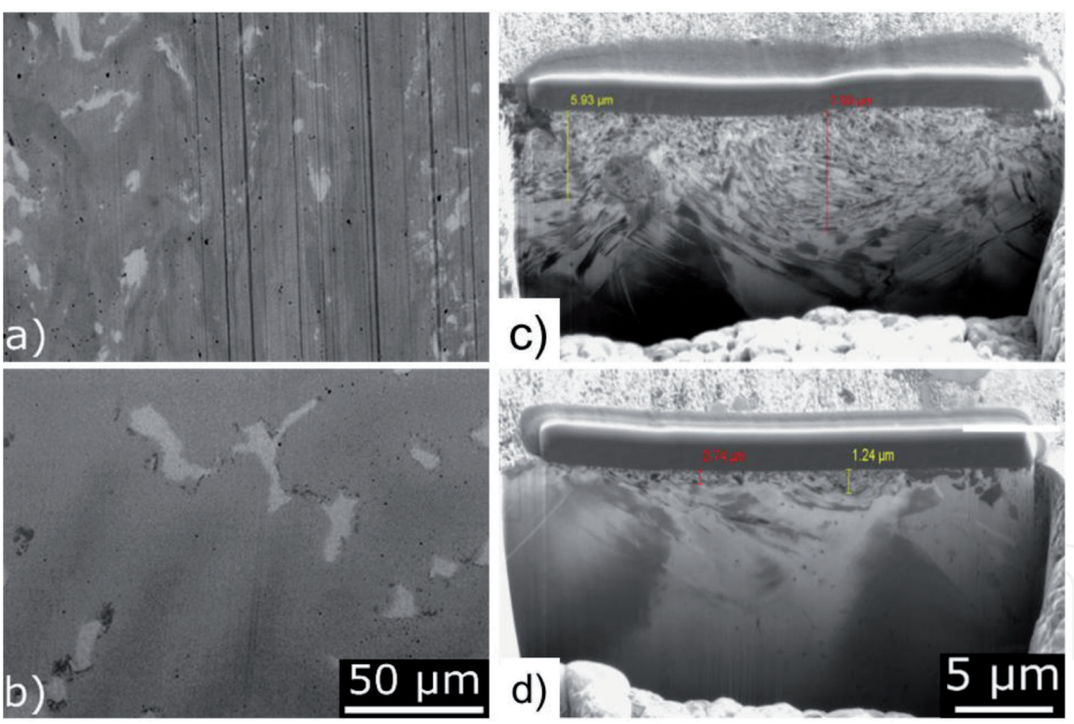

Figure 13.
Wear tracks on CuSn12Ni2: Top view SEM image - sliding direction going parallel to the vertical image edge a) conventional sample, b) LF sample; sub-surface microstructure in field ion image mode - sliding direction normal to the FIB cutting plane, c) conventional sample d) LF sample.

metallographic cross-section as it clearly reveals all phases. The LF surface appears even smoother than the CC surface. As the conventional cross sections indicated some edge effects, but did not enable a proper identification of the structure, only the respective FIB cuts, normal to the sliding direction, are given in **Figure 13c** and **d**. Here samples tested at a normal load of 240 N are examined as the wear volume differences are larger than for 100 N normal load. Both samples form a nanocrystalline layer during the sliding process. However, the thickness of this layer is clearly larger for the CC version with about 8 µm compared to 1.2 µm for LF. As the CC samples

had higher wear volumes, this layer does not seem to have wear protective effect, at least under the conditions investigated here. The nanocrystalline layer is not homogeneously thick, but rather shows a wavy interface in both studied cast structures. The average grain size within the nanocrystalline layer with about 250 nm seems to be constant over the thickness and in both samples. Potentially there are even smaller grains, but they cannot properly be resolved in SEM pictures.

5. Discussion

In lubricated reciprocating sliding contacts, all the studied copper alloy variants exhibited different tribological performance, if the microstructure was modified by changes in the production route. For the chosen loading conditions, the coarser and softer microstructures showed superior tribological performance compared to the finer grained and harder materials. Wear was pronouncedly reduced and friction coefficient levels of the run-in friction pairs were lower too for the softer variants of each alloy. This basic finding applies to dendritic cast structures as well as to globular structures.

In this study we compare the production routes MIM versus continuous casting followed by a massive forming step and lost foam casting versus continuous casting. MIM and LF both result in microstructures that are significantly coarser than the ones obtained through conventional processes. Thus these larger grained microstructures exhibit lower mechanical strength. Nevertheless, they showed to be more wear resistant than their smaller grained version from conventional processes. The effect was most pronounced for CuSn8 lubricated with non-additivated base oil SN150. This observation does not follow the conventional assumption that harder materials result in higher wear resistance, which follows the most common wear law of Archard and relates wear volume inversely proportional to macroscopic hardness [6]. As a consequence, small grained microstructures which result in higher tensile strength according to the Hall–Petch relation [16] are usually expected to be more wear resistant. Typically, only the initial or bulk material properties and microstructures are measured and taken into account [1].

In the present sliding systems, the detected wear volume of the initially coarse-grained structure and thus softer version of the alloy was significantly lower for both studied alloys and differed by factor of 2 for CuNi9Sn6 and by a factor of 2.5 for CuSn8. For the dendritic cast structures of the alloy CuSn12Ni2 the same effects on wear could be observed, but reduction was less pronounced. This can be attributed mainly to the use of additivated oil in order to be closer to the real application, yet, additives may contribute to a formation of a chemical wear protective tribofilm.

The analysis of the near-surface zones revealed the formation of a tribologically transformed layer and a mechanical mixed layer lying on top of the contact surface. Such a behaviour is well-known in tribology, but phenomenological descriptions of such microstructural changes often prevail [7, 25]. Few studies treat the effect of these layers on wear [26], or friction [27] More recent studies focus on the internal structure of the subsurface zone like the formation of a fibre texture [27] and/or the development of multiple grain structures, which split up in nano and micrometre sized grains [28]. Kapoor et al. [26] attribute the modified wear rates observed for different loading conditions to the different mechanical properties of these layers, independent of their genesis. Following Hall–Petch and Archard, a formation of a more fine-grained microstructure in the subsurface zone is expected to lead to local hardening and consequently to an increase of wear resistance.

However, the current study showed that the samples forming a thicker and more pronounced fine-grained zone exhibited higher wear than their chemically identical equivalents produced by MIM and LF, respectively. Typically, literature does

not cover the role of the material itself or different initial microstructures on wear and friction. As the most prominent difference between the chemically identical samples characterised here can be seen in the initial grain sizes, it was presumed to be a key influencing factor.

For the MIM version of CuSn8 the EBSD scans showed that the large grains react individually to the stress imposed during sliding and some accumulate plastic strain by an extremely localised work hardening processes. The local extension of the hardening is below or equal the single grain size. According to the EBSD results, the lattice orientation of grains exhibiting hardening is substantially different from neighbouring orientations. Thus, the number of their potential gliding planes with low Schmidt factors [29] differs a lot. The number of available slip planes is regarded as the main reason for the inhomogeneity of strain accumulation along the contact surface. Grains showing internal strains in the EBSD scans are assumed to have offered more slip systems with low Schmidt factors, with respect to the sliding direction, than the grains showing no enhanced defect density. If dislocation gliding is possible, the crystallographic lattice can take up strain and will partially rotate. If not, parts of the grain will be abraded directly with hardly any defect formation. The resulting enhanced hardening over a depth of 20 μm below the surface reaching up to 1.5 GPa was proven with nano-indentation measurements (**Figure 12**) for CuSn8. The EBSD scan illustrates that some grains take up plastic strain via local lattice rotations but form no new grain boundary. Quantitative analysis of SAGB or kernel average misorientation (KAM) are not depicted, because the large grains resulting from the MIM process revealed no substructure formation during sliding. The mechanically mixed layer found in patch-like structures on the surface could not be studied by EBSD as the misorientation was too high to identify grain structures. The nature of this layer would have to be verified in detailed TEM analyses in the future.

The TTL and the mechanically mixed patches are considered as two independently forming features (**Figure 14**), which both have the capability to reduce wear. The mechanically mixed layer presumably distributes the normal load and thus reduces the contact stress. The local hardening – though inhomogeneous – may postpone the detachment of wear particles as described in [30]. Surprisingly, we found no mechanical mixed layer on the small-grained structures with high initial twin densities (**Figure 9a**) after identical loading.

In contrast to the MIM version the initial grain structure of the conventional CuSn8 was fine-grained and exhibits very high twin densities. Such a highly deformed microstructure can hardly take up further plastic strain and the local work-hardening potential is low. Consequently, no TTL could be observed in the EBSD scans and the microstructure does not appear to adapt during sliding, but seems to be worn off immediately during sliding.

The dendritic cast alloy CuSn12Ni2 forms a nanocrystalline surface layer, which is similar to the ultra-nanocrystalline layer described for a Ni-alloy by [27].

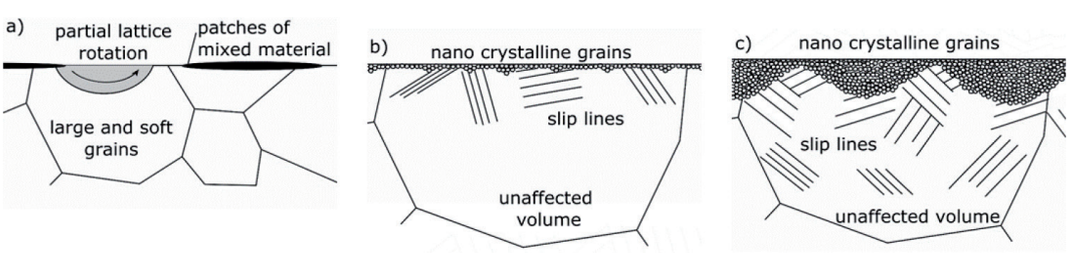

Figure 14.
Principal sketch of tribologically transformed zone beneath the surface a) partial grain rotation and tribolayer patches of mixed material b) formation of a thin layer of nanocrystalline grains accompanied by slip lines and twins, c) thicker nanocrystalline zone in vortex shape together with higher density of slip lines and twins formed also in larger depths.

We again refer to it as TTL. However, under loading conditions as those in the present study, this nanocrystalline layer was thicker for the finer structure resulting from continuous casting and very thin for the softer LF structure with large dendrites ranging over several hundred μm. Therefore, the nanocrystalline layer appears to be not beneficial for higher wear resistance.

Based on these observations we set up the following hypothesis for increased wear resistance of chemically equal, but softer, microstructures. Large grains without or with low initial defect densities can work-harden if the surface grains are appropriately oriented, i.e. so that the Schmidt factor of easy slip planes is low – (111) in the cubic systems of the study. For increased wear resistance, a near-surface layer has to take up plastic strains originating from the external stress state during the sliding process. This layer can form through local rotation of surface grains, as illustrated in **Figure 14**. For large grains, such as in the present study, where the grains have an average equivalent diameter of up to 250 μm, only partial rotation of grains occurs. Although the local grain rotations are rather inhomogeneous over the contact area, as many grains do not participate in local lattice rotations, this zone is relevant for the macroscopically observed wear volume and thus referred to as TTL. If the individual grains are saturated in defect densities, the surface near zone cannot work-harden and, as a consequence, the critical stresses for delamination or detachment of wear particles are much lower, wear occurs earlier and wear rates are higher.

Classical hardening through annealing processes and spinodal precipitations, which are found in CuNi9Sn6 can further reduce the wear volume compared to the non-hardenable CuSn8 as well as compared to the MIM version as shown in **Figure 5**. In the MIM version, the grain boundaries are facetted due to γ precipitation of length up to 2 μm at the grain boundaries, which is accompanied with a matrix depletion in the vicinity of the boundary. During heat treatment these precipitations at the boundaries dissolve and only lamellar phases within the grains and small intragranular precipitates form evenly distributed in the grains. The wear and friction result indicate that the latter structure is superior to adapt to the sliding process. Yet, the precipitation structure and distribution within the grains proved to be irrelevant for wear as well as friction. This indicates that the matrix composition and its element distribution determine the ability of a material to resist abrasion.

In the case of dendritic structures, the TTL comprises a nanocrystalline zone (**Figure 14**) with grain sizes ranging from 100 nm to 300 nm. Again, the thickness of this zone is inhomogeneous with "pockets" of nanocrystalline zones with an extension of about 20 μm below the surface (**Figure 13c** and **d**). As this characteristic is the same for the large grained LF and the finer grained CC sample, the wavy interface could be either a result of the large dendrite thickness and coarse grains or an effect of a periodic pattern of the contact stress state.

Still the differences of the respective maximum thicknesses are significantly different with 8 μm for CC and 1.2 μm for LF. The formation mechanism of such nanocrystalline grains is not entirely clear. [27, 30] compare the sliding process to rolling and torsion processes and claim that the near-surface textures are typical rolling textures. As the matrix of the MIM CuSn8 as well as the CuSn12Ni2 matrix, are both bronze metal matrix lattices, the local rotation found in CuSn8 could be an early status followed by formation of nanocrystalline grains.

The nanocrystalline layer found in LF samples resembles the non-continuous layer described in [28], referred to as nanostructured mixing layer (NML) and dynamic recrystallised layer. They show that these small grains form during the sliding contact and that the kinetics are different for different initial microstructures. The coarse-grained structures show higher wear rates which is not in line with our results on copper-based alloys. We found that the nanocrystalline layer is thicker for smaller-grained initial structures. However, the idea that not the

hardness of the initial microstructure determines wear resistance, but the ease with which the nanocrystalline layer can be peeled-off during sliding, seems to be an appropriate explanation for the wear behaviour of the conventional CuSn12Ni2 version forming thick nanocrystalline layers.

6. Conclusions

Innovative material production processes are usually associated with lower mechanical strength and with inferior performance. They lack trust by designers as they suffer comprehensive characterisation, especially tribological performance properties. In the current study, the technology route metal-injection moulding (MIM) and lost foam casting (LF) are applied to well-known commercial bronze alloys. The alternative routes resulted in more ductile and softer materials, but proved to be superior in terms of wear and even showed tendencies for lower friction levels under equal configurations and loadings.

A detailed characterisation executed using SEM, nanointendation as well as EBSD techniques revealed that all samples formed a tribologically transformed layer (TTL) beneath the contact surface, but that the extent of this layer was pronouncedly different. The following observations can be summarised for the current study:

- The thickness of the formed nanocrystalline layer depends on the material production route
- Thicker nanocrystalline layers do not enhance wear, but increase wear.
- Thus, grain refinement as a hardening mechanism does not go along with classical Archard approaches for increasing wear resistance via increasing hardness. The found nanocrystalline layer requires lower shear forces on the grains to be removed and this results in decreased macroscopic friction coefficients.
- The tribolayer, which showed to be a presumable amorphous mechanically mixed layer, forms independently of the TTL on MIM samples and was observed on samples showing lower wear than equivalently loaded conventionally produced variants.
- Large grained initial microstructures, produced by e. g. MIM, exhibit partial lattice grain rotation, which increases hardness very locally and were only observed on samples with lower wear.

Finally, we present a hypothesis for the formation timeline of nanocrystalline zones. Starting with local lattice grain rotation, followed by a monolayer on nanocrystalline grain layer accompanied with slip band and twin formation beneath and finally a thick nanocrystalline layer with a vortex structure. Based on the observation, we postulate that higher alloyed materials are more prone to local lattice rotation and defect formations such as twins and thus form a nanocrystalline zone more easily and quicker under the same loading conditions.

Acknowledgements

Topics presented are based on research projects with support by the Austrian COMET program (project XTribology, no. 849109, project InTribology, no. 872176)

and by the respective program management institutions, viz. the Austrian Research Promotion Agency (Österreichische Forschungsförderungs-Gesellschaft mbH – FFG), on behalf of the Federal Government, as well as proportionately by the Governments of Niederösterreich, Vorarlberg, and Wien. We are as well grateful to the involved company partners and scientific partners for their financial support and for the fruitful cooperation.

Author details

Ulrike Cihak-Bayr[1*], Robin Jisa[2] and Friedrich Franek[1]

1 AC2T research GmbH, Wiener Neustadt, Austria

2 Österreichische Tribologische Gesellschaft, Wiener Neustadt, Austria

*Address all correspondence to: ulrike.cihak-bayr@ac2t.at

References

[1] Suffian S, Dzombak R, Mehta K. Future directions for nonconventional and vernacular material research and applications. Nonconv. Vernac. Constr. Mater., Elsevier; 2016, p. 63-80. DOI:10.1016/B978-0-08-100038-0.00003-2.

[2] Marini D, Cunningham D, Corney JR. Near net shape manufacturing of metal: A review of approaches and their evolutions. Proc Inst Mech Eng Part B J Eng Manuf 2018;232:650-69. DOI: 10.1177/0954405417708220.

[3] Khodai M, Parvin N. Pressure measurement and some observation in lost foam casting. J Mater Process Technol 2008;206:1-6. DOI: 10.1016/j.jmatprotec.2007.11.309.

[4] Shivkumar S, Wang L, Apelian D. The lost-foam casting of aluminum alloy components. JOM 1990;42:38-44. DOI: 10.1007/BF03220435.

[5] Li G, Jiang W, Fan Z, Jiang Z, Liu X, Liu F. Effects of pouring temperature on microstructure, mechanical properties, and fracture behavior of Al/Mg bimetallic composites produced by lost foam casting process. Int J Adv Manuf Technol 2017;91:1355-68. DOI: 10.1007/s00170-016-9810-y.

[6] Archard JF. Contact and rubbing of flat surfaces. J Appl Phys 1953;24:981-8. DOI: 0.1063/1.1721448.

[7] Rigney DA. Transfer, mixing and associated chemical and mechanical processes during the sliding of ductile materials. Wear 2000;245:1-9. DOI: 10.1016/S0043-1648(00)00460-9.

[8] Argibay N, Chandross M, Cheng S, Michael JR. Linking microstructural evolution and macro-scale friction behavior in metals. J Mater Sci 2017;52:2780-99. DOI: 10.1007/s10853-016-0569-1.

[9] Greiner C, Liu Z, Strassberger L, Gumbsch P. Sequence of Stages in the Microstructure Evolution in Copper under Mild Reciprocating Tribological Loading. ACS Appl Mater Interfaces 2016;8:15809-19. DOI: 10.1021/acsami.6b04035.

[10] Equey S, Houriet A, Mischler S. Wear and frictional mechanisms of copper-based bearing alloys. Wear 2011;273:9-16. DOI: 10.1016/j.wear.2011.03.030.

[11] Perret J, Boehm-Courjault E, Cantoni M, Mischler S, Beaudouin A, Chitty W, et al. EBSD, SEM and FIB characterisation of subsurface deformation during tribocorrosion of stainless steel in sulphuric acid. Wear 2010;269:383-93. DOI: 10.1016/j.wear.2010.04.023.

[12] Mola J. Considerations in the Design of Formable Austenitic Stainless Steels Based on Deformation-Induced Processes. Austenitic Stainl. Steels - New Asp., InTech; 2017. DOI: 10.5772/intechopen.70939.

[13] Zhao C, Zhou J, Mei Q, Ren F. Microstructure and dry sliding wear behavior of ultrafine-grained Co-30 at% Cr alloy at room and elevated temperatures. J Alloys Compd 2019;770:276-84. DOI: 10.1016/j.jallcom.2018.08.092.

[14] Liu J, Yang S, Xia W, Jiang X, Gui C. Microstructure and wear resistance performance of Cu-Ni-Mn alloy based hardfacing coatings reinforced by WC particles. J Alloys Compd 2016;654:63-70. DOI: 10.1016/j.jallcom.2015.09.130.

[15] Sinclair CW, Poole WJ, Bréchet Y. A model for the grain size dependent work hardening of copper. Scr Mater 2006;55:739-42. DOI: 10.1016/j.scriptamat.2006.05.018.

[16] Schiøtz J, Jacobsen KW. A maximum in the strength of nanocrystalline copper. Science. 2003;301:1357-9. DOI: 10.1126/science.1086636.

[17] Zhao JC, Notis MR. Spinodal decomposition, ordering transformation, and discontinuous precipitation in a Cu-15Ni-8Sn alloy. Acta Mater 1998;46:4203-18. DOI: 10.1016/S1359-6454(98)00095-0.

[18] Virtanen P, Tiainen T, Lepistö T. Precipitation at faceting grain boundaries of Cu-Ni-Sn alloys. Mater Sci Eng A 1998;251:269-75. DOI: 10.1007/s10853-015-9341-1

[19] Jisa R, Ristic A, Brenner J, Lebersorger T, Ilo S, Neumayer H. Effectiveness of lubricant additives for copper-alloy-steel sliding contacts. Lubr Sci 2010. DOI: 10.1002/ls.118.

[20] Jisa R, Laumann S, Cihak-Bayr U, Tomastik C, Eberle R, Keppeler M. Tribological properties of MIM manufactured copper alloys. Tribol - Mater Surfaces Interfaces 2014;8. DOI: 10.1179/1751584X14Y.0000000064.

[21] Cihak-Bayr U, Jisa R, Franek F. Tribological Behaviour of MIM Produced Copper Alloys 2015;273:824187.

[22] Standard Test Method for Determining Extreme Pressure Properties of Lubricating Greases Using A High-Frequency , Linear-Oscillation (SRV) 1985:7-10. DOI: 10.1520/D7421-11.2.

[23] Mason JK, Schuh CA. Representations of Texture. Electron Backscatter Diffr. Mater. Sci., Boston, MA: Springer US; 2009, p. 35-51. DOI: 10.1007/978-0-387-88136-2_3.

[24] Nolze G, Jürgens M, Olbricht J, Winkelmann A. Improving the precision of orientation measurements from technical materials via EBSD pattern matching. Acta Mater 2018;159:408-15. DOI: 10.1016/j.actamat.2018.08.028.

[25] Cai W, Mabon J, Bellon P. Crystallographic textures and texture transitions induced by sliding wear in bronze and nickel. Wear 2009;267:485-94. DOI: 10.1016/j.wear.2008.11.016.

[26] Kapoor A, Franklin FJ. Tribological layers and the wear of ductile materials. Wear 2000;245:204-15. DOI: 10.1016/S0043-1648(00)00480-4.

[27] Padilla HA, Boyce BL, Battaile CC, Prasad S V. Frictional performance and near-surface evolution of nanocrystalline Ni-Fe as governed by contact stress and sliding velocity. Wear 2013;297:860-71. DOI: 10.1016/j.wear.2012.10.018.

[28] Yao B, Han Z, Lu K. Correlation between wear resistance and subsurface recrystallization structure in copper. Wear 2012;294-295:438-45. DOI: 10.1016/j.wear.2012.07.008.

[29] Greiner C, Gagel J, Gumbsch P. Solids Under Extreme Shear: Friction-Mediated Subsurface Structural Transformations. Adv Mater 2019;31:1806705. DOI: 10.1002/adma.201806705.

[30] Rainforth WM. Microstructural evolution at the worn surface: A comparison of metals and ceramics. Wear 2000;245:162-77. DOI: 10.1016/S0043-1648(00)00476-2.